Tailoring Exciton Dynamics by Elastic Strain-Gradient in Semiconductors

Xuewen Fu, Cong Su, Qiang Fu, Xinli Zhu, Rui Zhu, Chuanpu Liu, Zhimin Liao, Jun Xu, Wanlin Guo, Ji Feng,* Ju Li,* and Dapeng Yu**

Precise modulation of electronic structures and electrodynamics at atomic scale is an essential element for improving the physical and chemical properties of semiconductors in photovoltaics,[1–3] photodetection,[4] photocatalysis,[5] and field-effect transistors.[6,7] Elastic strain engineering can be an effective route for tuning material properties fast, reversibly, and continuously. Small dimensionality renders microwires (MWs) or nanowires (NWs) the ability to withstand a larger elastic deformation compared with their bulk counterparts,[8–10] therefore, it is possible to tune the physical and chemical properties dramatically by elastic strain engineering in low dimensional systems. For example, strain-based silicon technology has been widely utilized commercially for enhancing carrier mobility in CMOS transistors.[6] Recently, experimental progresses have shown the significant energetic red-shift of the near-band-edge (NBE) emission in bent ZnO NW[11–16] and CdS NW,[17] leading to a proposed flexoelectronic effect[14,17] in semiconductors. The energetic red-shift has also been experimentaly observed in uniaxial strained ZnO[18] and GaAs[19] NWs by cathodoluminescence (CL) or photoluminescence (PL) studies. Furthermore, the bending deformation in ZnO MWs/NWs has given rise to novel nanogenerators[20,21] and opto-piezotronic devices.[22,23] Most recently, over sixty years after the initial conception of the deformation potential,[24–26] it has been theoretically proposed that an inhomogeneous strain field created in a semiconductor atomic membrane can induce spatial concentration of photoexcited carriers.[27] However, tuning the electrodynamics by elastic inhomogeneous strain has yet to be further established both theoretically and experimentally.

In this work, by combining theoretical and experimental approaches, we illustrate that by imposing elastic strain gradient we can tailor the dynamics of excitons in semiconducting ZnO MWs. The key role of an inhomogeneous elastic strain distribution is to give rise to a continuously varying electronic band structures profile, thus the continuously varying exciton potential, which induces an effective built-in field that drives the excitons to transport in side MWs. Our work is an initial demonstration of the paradigm of elastic strain-gradient for tailoring exciton dynamics, further revealing the underlying mechanism of the proposed flexoelectronic effect[14,17] in semiconductors.

Elastic strain corresponds to a relative displacement of atoms in material, where a shift of energy bands is correlated to the change of electronic cloud overlap between atoms.[24,27] By imposing pure bending deformation on a ZnO MW, we can precisely create an inhomogeneous strain field with a uniform radial strain-gradient. As schematically shown in **Figure** 1a, the tangential strain along the hexagonal axis (0001) varies linearly from the belly (inner side) to the back (outer side), separated by an intermediate neutral plane. Previous computational and experimental results demonstrate that, in ZnO crystals, tensile and compressive strains along (0001)-axis can linearly reduce and increase the bandgap,[12,28–30] respectively. Therefore the bandgap are expected to show a continuous spatial variation from belly to back in a purely bent ZnO MW.

We performed density functional theory calculations on the electronic energy bands of different strained (*c*-axis) ZnO crystal (see Methods). The strain-dependent distributions of the electronic energy bands along the cross section of a purely bent ZnO MW (1.7 μm in diameter) is shown in Figure 1b. Both the valence band maximum (VBM) and conduction band minimum (CBM) linearly shift downwards from the belly side towards back side (see Figure 1b), where CBM is more sensitive than VBM to elastic strain, and the deformation potentials of CBM and VBM are $k_C = -52.7$ meV/1% and $k_V = -21.3$ meV/1%, respectively. Correspondingly, the bandgap decreases linearly along radial direction from the belly to the back side as $\Delta E_{gap} = (k_C - k_V)\varepsilon$ eV (see Figure 1c). Therefore, a red-shift of NBE luminescence is expected from the back side of purely bent MW, and a blue-shift from the belly side. Since the exciton binding

Xuewen Fu,[+] Qiang Fu, Xinli Zhu, Rui Zhu, Chuanpu Liu, Zhimin Liao, Jun Xu, Dapeng Yu
State Key Laboratory for Mesoscopic Physics and Electron Microscopy Laboratory, School of Physics Peking University, and Collaborative Innovation Center of Quantum Matter
Beijing, 100871, China
E-mail: yudp@pku.edu.cn
Cong Su,[+] Ji Feng
International Center for Quantum Materials
School of Physics
Peking University
and Collaborative Innovation Center of Quantum Matter
Beijing, 100871, China
E-mail: jfeng11@pku.edu.cn
Wanlin Guo
Key Laboratory of Intelligent Nano Materials and Devices of MOE
Institute of Nano Science
Nanjing University of Aeronautics and Astronautics
29 Yudao Street, Nanjing, 210016, China
E-mail: wlguo@nuaa.edu.cn
Cong Su,[+] Ju Li
Department of Nuclear Science and Engineering and Department of Materials Science and Engineering, Massachusetts Institute of Technology
Cambridge, Massachusetts, 02139, USA
E-mail: liju@mit.edu
[+]These authors contributed equally to this work.

DOI: 10.1002/adma.201305058

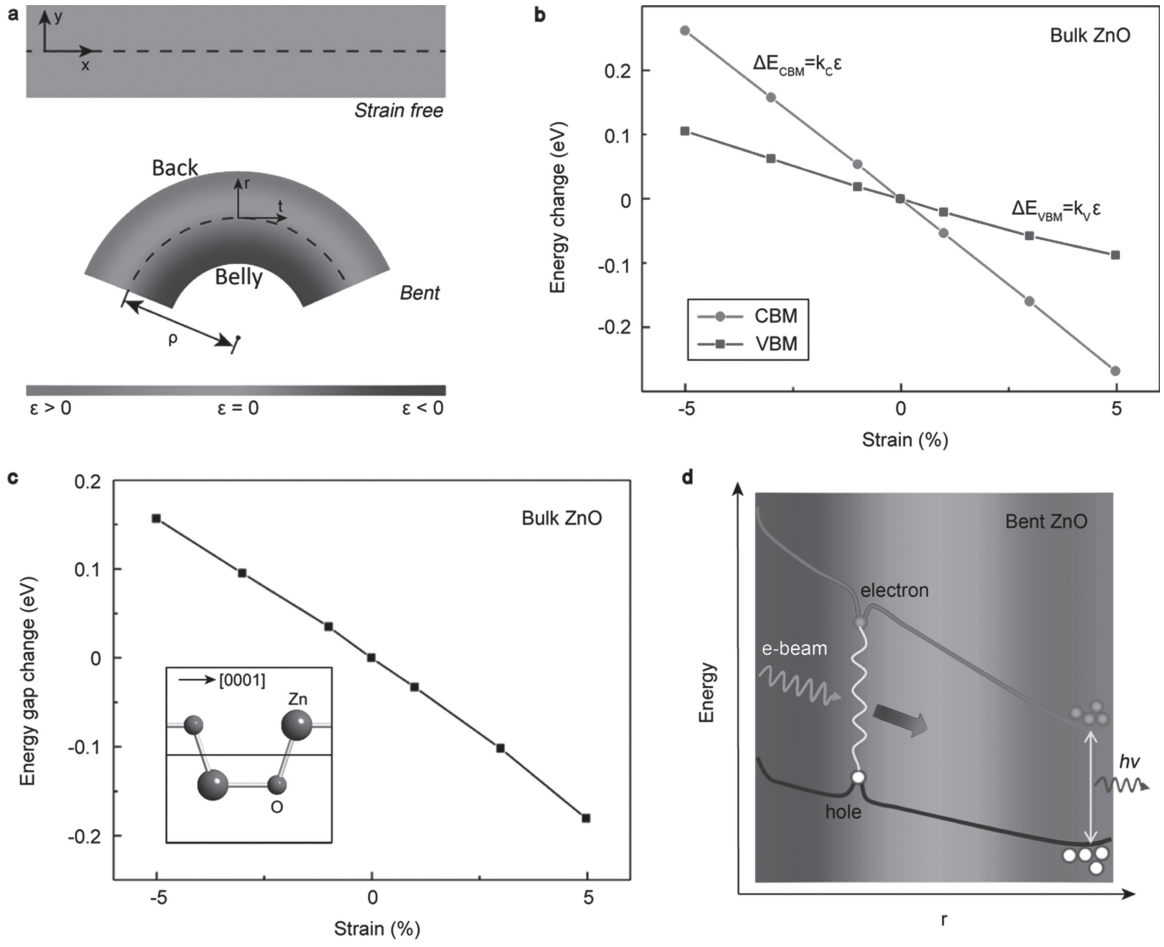

Figure 1. Introduction of pure bending strain and strain-dependent electronic and optical properties of ZnO MW in pure bending deformation. (a) A schematic configuration of a strain-free (upper) and a purely bent (lower) ZnO MW. The radius of curvature of the purely bent MW is denoted as ρ in the graph. (b) The energy change of conduction band minimum (CBM) and valence band maximum (VBM) as a function of the c-axis strain in bulk ZnO. The slope of CBM is $k_C = -52.7$ meV/1% and that of VBM is $k_V = -21.3$ meV/1%. (C) The energy bandgap change as a function of the c-axis strain in bulk ZnO. Inset: the primitive cell of a bulk ZnO. (d) The transport mechanism of excitons in the cross section of a purely bent ZnO MW. The red and blue colors in Figure 1a and 1d represent the local tensile and compressive strain, respectively.

energy is up to 60 meV in ZnO, it is reasonable to assume that the excitons would not split into free electrons and holes in the pure bending strain field. Due to the continuous variation of the bandgap, a continuous varying potential of excitons in the purely bent ZnO MW can be formed by the elastic strain-gradient. Excitons generated by steady-state optical or electron beam excitation can migrate towards the back side with lower exciton potential before recombination, as schematically shown in Figure 1d.

For simplicity, we propose a two-dimensional phenomenological model to simulate the exciton dynamics in a ZnO MW under pure bending deformation. Under steady electron beam excitation in one confined region, the dynamical equation for the excitons reads

$$\partial_t n(rt) + \nabla \cdot \mathrm{j}(rt) = g(rt) - \tau^{-1} n(rt) \tag{1}$$

where $n(\mathbf{r}t)$ and $\mathbf{j}(\mathbf{r}t)$ are the *number* density and flux of the excitons, respectively; $g(\mathbf{r}t)$ is the generation rate; τ is the recombination lifetime of the excitons, taking into account various relaxation pathways. The flux $\mathbf{j}(\mathbf{r},t)$ is

$$\mathrm{j} = D\nabla n - \mu n \nabla \phi_{e.s} \tag{2}$$

where the first term correspond to the diffusion of excitons, and the second term correspond to the drift current induced by an effective potential. D is the diffusion coefficient of excitons; $\mu = D/k_B T$ is the mobility of excitons; $\varphi_{e.s.}(\mathbf{r})$ is the local exciton potential in the cross section of the purely bent ZnO MW (see Supporting Information for more details). In our simulation, the MW is 1.7 μm in diameter and 1.17% μm $^{-1}$ in strain-gradient (defined as the inverse of the radius of bending curvature).

Figure 2a and Figure 2b show the side and top views of exciton distribution within one cross section in the pure bending region with different static electron exciting locations (considering the high spatial resolution of CL in experiment) from tensile side to compressive side (subfigures from down

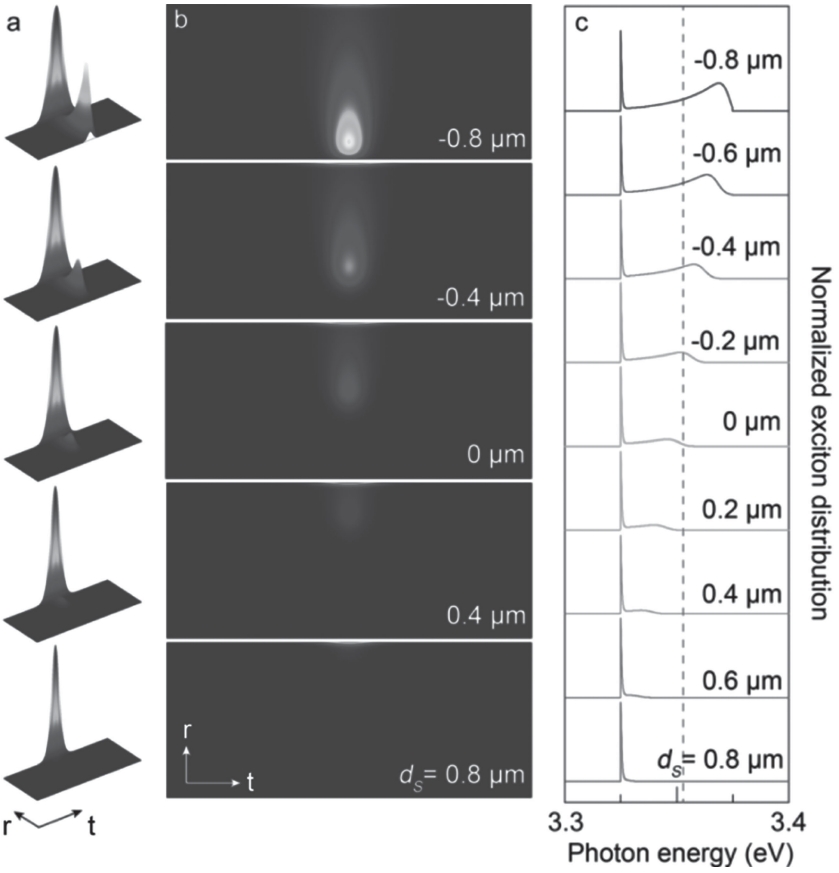

Figure 2. Simulation results of the excitons distribution in the cross section of a purely bent ZnO MW with elastic strain-gradient of $g = 1.17\%\ \mu m^{-1}$. (a) and (b) Three-dimensional views and top views of exciton distribution in a cross section of the purely bent ZnO MW under elastic strain-gradient of $g = 1.17\%\ \mu m^{-1}$ with different electron beam exciting locations from tensile side to compressive side (bottom to up). *t* direction is set along c-axis of the pure bent MW, and the direction perpendicular to the *r*-*t* plane represents the normalized concentration of excited states. The electron beam exciting location with respect to the neutral surface is denoted as d_S. The width of the MW is 1.7 μm, where the top and bottom boundaries of pure bent microwire are at the places of d_S = 0.85 and -0.85 μm, respectively. (c) The normalized exciton distribution as a function of photon energy with electron beam exciting location moving from tensile side to compressive side (bottom to up). The pink dashed line indicates the original strain-free position of the NBE emission photon energy in ZnO MW.

to top in Figure 2a and Figure 2b), respectively. Here we have mapped the corresponding points in the bending wire to a straight section as an approximation, which is valid since the radius of curvature of the bent wire is much larger than the wire diameter. Interestingly, when the electron beam is focused at the tensile side of the MW (d_s = 0.8 μm and 0.4 μm, where d_s means the distance of electron exciting location with the neutral surface hereinafter), nearly all the excitons stay localized; whereas the foci of electron beam move toward the compressive side, we see clearly that the exciton density still peaks at the tensile edge due to the exciton drift, leaving a streak toward the electron incident point (d_s = –0.4 μm and –0.8 μm). If we move the exciting electron source from the back to belly side of MW step by step, the collected spectra of the whole cross section should exhibit a dominant constant red-shifted emission peak, and a source-track weaker and broader peak with higher photon energy, as schematically shown in Figure 2c.

To confirm our theoretical analysis, we carry out high spatial and energy resolution CL characterization on ZnO MWs with high quality under pure bending at 5.5 K, with a specially designed standard four-point-bending (4PB) setup (see Method Section).[31] **Figure 3**a schematically shows the line-scanning CL measurement procedure. In these measurements, the electrons are injected step by step along a cross section in the pure bending region of the ZnO MW. Figure 3b schematically illustrates the strain distribution in a ZnO wire in such a 4PB setup, in which the four pillars divide the wire into five segments. The middle segment is in a pure bending state, with the c-axis strain distributing linearly from inner side to outer side as $\varepsilon_{tt} = r/R$ ($|r| \le d/2$), where d is the diameter of the wire, and R the radius of curvature of the local neutral plane. Here, we adopt a local *r*-*t* coordinates (see Figure 3b), where r and t are the mutually perpendicular local radial and tangential directions (r is measured from the neutral plane). Figure 3c shows the typical top-view SEM image of a 4PB ZnO MW (2.8 μm in diameter).

The CL spectra measurements are performed at 5.5 K in a liquid helium flow cryostat, under which only one intensive NBE peak, corresponding to a neutral donor bound exciton D^0X_A,[32,33] is dominant around 3.359 eV for strain-free ZnO wires (see Figure S2, Supporting Information). Figure 3d shows four sets of CL spectra, each corresponding to a cross section of the ZnO MW. One set of spectra are collected for a cross section in the straight region ("I" Figure 3c). Three other sets of spectra correspond to three cross sections in the middle segment ("II", "III" and "IV", respectively). Clearly, the line-scanning CL spectra at "II", "III" and "IV" are identical, confirming that the middle segment of the 4PB MW is indeed in the elastic purely bent state. The line-scanning CL spectra collected from the cross section in the bending region of the wire are still dominated by the D^0X_A luminescence peak, but are clearly red-shifted compared with the emission peak in the strain-free region by 33 meV. Another key observation here is that two weaker but identifiable peaks (labelled as M and R) with higher energies emerge with the electron injection spot moving towards the inner side. The energy of M peak stays almost unchanged, while that of R peak linearly increases.

This experimental result is in good agreement with the theoretical simulation presented in Figure 2. The only major difference between experiment and simulation is that, there are three peaks (one intensive peak and two weak peaks) when electron beam is focused on the belly side of the bent wire, whereas only two peaks (one intensive peak and one weak peak) are found in the simulation results. This additional peak M in experimental

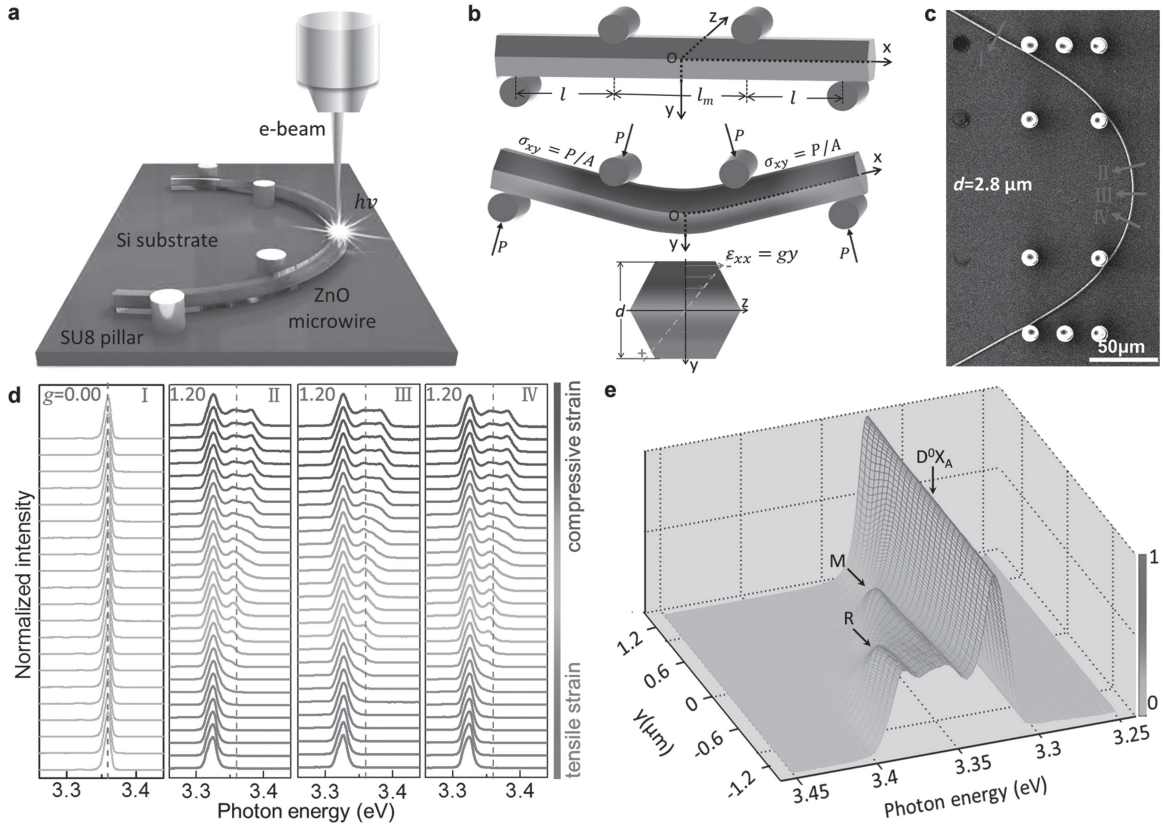

Figure 3. Schematic diagram of CL measurement and strain distribution in a 4PB ZnO MW. (a) Top-view SEM image of a typical 4PB ZnO MW with diameter of d = 2.8 μm. (b) Distribution of strain ε_{tt} in a standard 4PB MW subjected to force P at the four points. The red and blue colors illustrate the tensile and compressive regions in the bent wire, respectively. The figure bottom insert shows the c-axis strain ε_{tt} distribution in the pure bending cross section. (c) Schematic diagram for line-scanning CL measurements on the pure bending region of a 4PB ZnO MW step-by-step from tensile to compressive edges. (d) Line-scanning CL spectra on the strain-free section "I" and from the pure bending region (section "II"-"IV") with constant strain-gradient g = 1.20% μm^{-1} at 5.5 K. The red and blue colors in the CL spectra represent the tensile and compressive strain, respectively. The pink dash lines indicate the original strain-free position of the NBE emission peak. (e) Three-dimensional graph of the NBE emission spectra (normalized in intensity) along the cross-section "III" of the 4PB ZnO MW.

spectra can be attributed to one of the whispering gallery mode (WGM) resonances that arise from the light internal reflection at the side facets within the hexagonal cross section of the MW.[34] It is a completely photonic characteristic and the position of the WGM is determined by the refractive index and diameter of the cross section. The assignment of peak M to the WGM is supported by two observations: (1) the peak stays almost unchanged for the same wire regardless of the position of the electron beam irradiation; and (2) the peak M changes with the diameter of the wire according to resonance condition of the WGM.

To further reveal the exciton dynamics behavior in a 4PB ZnO MW under different pure bending states, we carried out CL measurements on one same ZnO MW under three different strain-gradients: g_I = 0.00% μm^{-1} (ε_{tt}^{max} = 0.00%), g_{II} = 0.57% μm^{-1} (ε_{tt}^{max} = 0.48%) and g_{III} = 1.16% μm^{-1} (ε_{tt}^{max} = 0.98%), as shown by the 30°-tilted SEM images in **Figure** 4a from left to right. The line-scanning CL spectra collected from the same cross section under the three different pure bending states indicated by the pink arrows in Figure 4a are presented in Figure 4b. Similar to the line-scanning CL spectra results presented in Figure 3d, only one intensive constant red-shifted D^0X_A peak dominates the CL spectra at the whole cross section from tensile to compressive edges under different bending states. When the ZnO MW is bent from the strain-free state "I" into state "II" and state "III", $(D^0X_A)_I$ shifts to $(D^0X_A)_{II}$ and $(D^0X_A)_{III}$, with red shifts of 12.97 meV and 24.43 meV, respectively. Note that $(D^0X_A)_{II}$ has larger full width at half maximum than that of $(D^0X_A)_I$ and $(D^0X_A)_{III}$. This larger peak broadening is easy to be understood by our theoretical model: In state "II", the strain-gradient induced effective built-in field is not large enough to immediately drive the excitons to the edge of the back-side before they recombination. Consequently, the luminescence has a broad spectrum corresponding to a broader distribution of excitons in the cross section.

To have a comprehensive view of the NBE emission energy evolution from states "I" to "III", the spectra of all three bending states are displayed in Figure 4c. With the electron excitation spot moving to the compressive edge, the M peak enters a stable region with a nearly constant energy of 3.365 eV, while the R peak shows a gradual blue shift to 3.381 eV (see Figure S3 for more discussion). In accordance

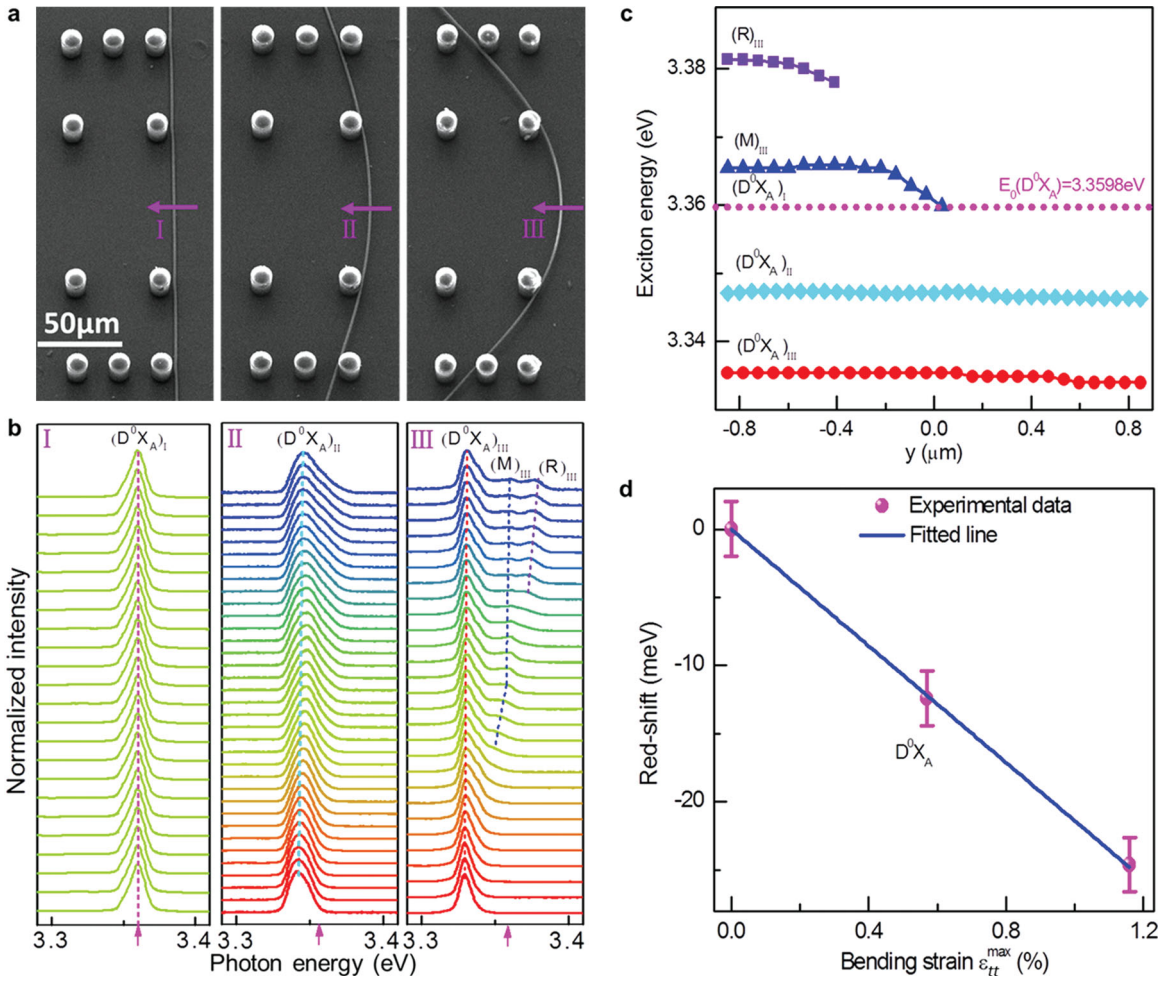

Figure 4. Red-shift of the NBE emission photon energy in a 4PB ZnO MW (d = 1.7 μm) under different elastic pure bending states at 5.5 K. (a) 30°-tilted SEM images of the same individual ZnO MW (d = 1.7 μm) in the 4PB setup before bending (left), bent to g_{II} = 0.57% μm^{-1} (middle) and to g_{III} = 1.16% μm^{-1} (right). The pink arrows indicate the CL line-scanning direction and the same studied cross section. (b) The collected line-scanning CL spectra from the same cross section under the three different pure bending states ("I", "III") shown in Figure 4a at 5.5 K. The red and blue colors represent tensile and compressive strain, respectively. The upward pink arrows at the bottom of the spectra indicate the original strain-free position of the NBE emission peak. (c) Positions of the NBE emission peaks with electron beam exciting spot moving along the cross-section at different pure bending states. $(D^0X_A)_I$: D^0X_A emission photon energy under the strain free state "I"; $(D^0X_A)_{II}$: D^0X_A emission photon energy under the first pure bending state "II" with g = 0.57% μm^{-1}; $(D^0X_A)_{III}$: D^0X_A emission photon energy under the second pure bending state "III" with g = 1.16% μm^{-1}; $(M)_{III}$ and $(R)_{III}$: emission photon energies of the weak M and R peaks under the second pure bending state "III" with g = 1.16% μm^{-1}. (d) Linear red-shift of the dominant emission (D^0X_A) photon energy of the NBE emission against the elastic pure bending strain. The linear fitting process in Figure 3d yields the bending deformation potential of –2.49 eV for the 4PB ZnO MW. The error bars of the data are determined by the energy resolution of the CL spectroscopy.

with our simulation result, the energy red shift of D^0X_A peak indeed varies linearly with the increasing bending strain, or strain gradient, also confirming the previously proposed flexoelectronic effect[14,17], as shown in Figure 4d. The linear fitting yields $\Delta E = kgd/2 = k\varepsilon_{tt}^{max}$ (without considering Poisson effect here), where $k = \partial(\Delta E)/\partial\varepsilon_{tt}^{max} = (d/2)\partial(\Delta E)/\partial g = -2.49$eV is the bending deformation potential of the purely bent ZnO MW. As the pure bending is different from hydrostatic and uniaxial compression, it is reasonable that the deformation potential obtained in our experiment is larger than that of Dietrich's experiments (–2.04 eV)[12] and smaller than that of Shan's pressure experiments (–3.92 eV).[29]

An issue that must be reckoned with is the possibility that the piezoelectric polarization induced built-in transverse electric field[35,36] should enter into the physics discussed here. In a bent ZnO wire, this bending deformation induced piezoelectric field would result in inhomogeneous band bending inside the ZnO MW. But as it amounts to an electrostatic potential which shifts or bends the valence and conduction bands equally, the piezoelectric field will not significantly alter the frequency of light emitted. Xu et al. attributed the net red-shift of the NBE emission photon energy in bent ZnO wires to the piezoelectric field modification of the photoexcited carriers.[15] When electron-hole pairs are generated in the bending region of the ZnO MWs, the transverse piezoelectric field could only influence the motions of separated electrons and holes. However, due to the strong exciton binding energy in ZnO, the generated electron-hole pairs prefer to stay coupled. The center-of-mass

force, which drives the motion of a neutral exciton, has vanishing coupling to the piezoelectric field, to the leading order. Fundamentally, the excitons are neutral particles which should not "care" about the Coulomb potential; it should be the strain-induced band gap or exciton potential change that the excitons "care" the most about.

Formalistically, an exciton's total energy is expressed as $E_g - E_B$. The gap energy E_g represents the energy difference between single electron injection (electron affinity) and single hole extraction (ionization potential) at well-separated locations in the material. The exciton binding energy E_B is the energy reduction when the electron and hole are brought into proximity. Since band-bending due to electric field has no effect on the band gap at a given location, we have argued that E_g is independent of the electric field **E**, and only cares about the strain tensor ε :

$$E_g = E_g^{\text{ref.}} + \varepsilon : (\partial E_g + \partial \varepsilon)^{\text{ref.}} + \mathcal{O}(\varepsilon^2). \tag{3}$$

Here the electric field may be that of the piezoelectric polarization, $\mathbf{E} = \eta \mathbf{P}$, where η is the inverse dielectric constant of the material. On the other hand, E_B does care about **E** and ε :

$$E_B = E_B^{\text{ref.}} + \varepsilon : (\partial E_B / \partial \varepsilon)^{\text{ref.}} - \frac{1}{2}\alpha^{\text{ref.}} : \mathrm{EE} + \mathcal{O}(\varepsilon^2, \varepsilon \mathrm{E}^2), \tag{4}$$

where α^{ref} is the electric polarizability of the exciton, but since $E_B << E_g$ it is unlikely to contribute much. The total driving force **F** on exciton center-of-mass motion should therefore be

$$\mathrm{F} = -(\nabla \varepsilon) : (\partial E_g / \partial \varepsilon + \partial E_B / \partial \varepsilon)^{ref.} + \frac{1}{2}\alpha^{\text{ref.}} : \nabla \mathrm{EE} + \mathcal{O}(\nabla \varepsilon^2, \nabla \varepsilon \mathrm{E}^2) \tag{5}$$

where in the present work we only took the first-order term without the change in the exciton binding,

$$\mathrm{F} = -(\nabla \varepsilon) : (\partial E_g / \partial \varepsilon)^{\text{ref.}} \tag{6}$$

which is expected to be dominant in the drift-diffusion Equation (1), (2). Notice that in this general formal analysis, the polarization field only enters as second order terms.

To further verify that we are indeed dealing with mainly charge-neutral phenomena that does not couple strongly to the piezoelectric field, we also perform an experiment to measure the photo-current (bias of 0 V) across a purely bent ZnO wire under UV (325 nm) laser excitation, and found that there is essentially zero photocurrent. This is opposite to the expectation from a piezoelectric mechanism, where the polarization field should give rise to a photo-current.

Another issue has to be reckoned with is the discrepancy of the results reported in the previous works[11–16] and that in this work. In the previous results, the NBE luminescence spectrum linearly red shifts in the outer side and blue shifts in the inner side of the bent ZnO wire at higher temperature (81 K and 300K)[11–16]. This discrepancy can be reasonable understood by our theoretical analysis. As the exciton drift by strain gradient is strongly dependent on exciton mobility and its life time, due to the strong scattering effect and high nonradiative ratio at higher temperature, exciton would have very low mobility and short life time. Therefore, it is difficult to observe the exciton drift apparently at higher temperature. The exciton will recombine locally to luminescence and results in linearly red- and blue-shift of the NBE luminescence spectrum in outer and inner sides of the bent wire.

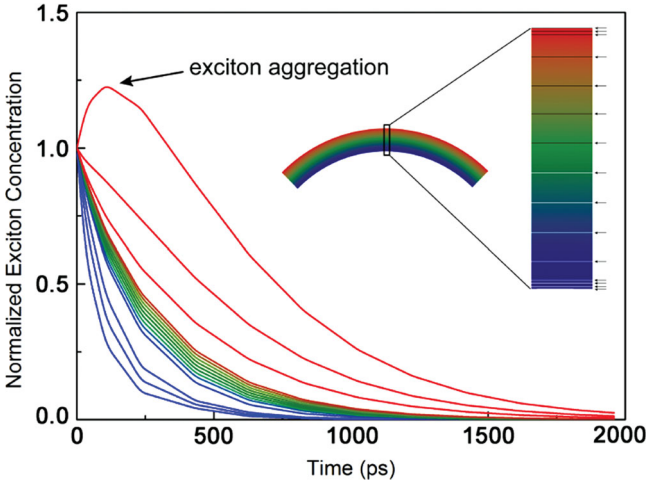

Figure 5. Time-dependent simulation result of exciton transport in purely bent ZnO MW in PL experiment with ultrafast laser excitation. The color of each line, representing the energy of the excitons, is in accordance with the strain distribution in MW, as shown by the inset figure. Fifteen groups of excitons with different energies are sampled on the cross section of the purely bent ZnO MW, as marked by lines in the inset color bar. The increase of the concentration near the back side of ZnO MW after t = 0 ps indicates the aggregation of exciton under the strain-gradient scheme.

The strain gradient induced exciton drift effect proposed herein may also be detected by ultrafast optical measurements. We carry out time-dependent simulations of the dynamical process of excitons in a time-resolved PL experiment. In this experiment, the entire bending cross section of the purely bent ZnO MW is excited by an optical pulse. We depict the simulated decay process of luminescence with the time evolution in **Figure** 5. The time evolution of luminescence intensity is remarkably different for different photon energies. The high-energy emission decays super-exponentially. The intensity of the low-energy emission undergoes an initial rise. This is a direct consequence of the exciton migration along the internal energy gradient. Therefore, ultrafast dynamics measurements with spectral and time resolution will be an interesting experiment, to directly reveal the detailed decay kinetics of the excitons in an inhomogeneous strain field.

The experimental evidence for exciton drift in the inhomogeneously strained semiconductor micro/nanowires should be of great potential for exciton condensation, lasing, photovoltaic conversion, and optical detection. The unique feature of these devices is that the emission photon energy and intensity, as well as the absorbent light frequency can be continuously tuned by varying the applied bending strain. The fabrication of these devices should be very simple, as the strain-gradient in semiconductor micro/nanowires can be easily and precisely tuned by controlling the bending curvature and specimen geometry.

In conclusion, through systematic high spatial and energy resolution CL investigations on purely bent ZnO MWs at 5.5 K, we find that the NBE emission spectra exhibit a dominant red-shift peak at the whole bending cross section and two weak higher energy emission subbands emerge when entering the compressive side. The experimental results are in excellent agreement with our simulations, which demonstrate that dynamics of excitons can be artificially tailored by the elastic strain gradient. An effective potential can be created by the strain gradient that directs the motion and concentration of the exciton towards the low energy region, leading to the proposed flexoeelctronic effect[14,17]. The physical mechanism we proposed is rather generic and applicable to most semiconductors, and can be widely used in broad band photovoltaic conversion and optical detection.

Methods

ZnO Microwires Growth: The synthesis of ZnO microwires was carried out in a horizontal quartz tube furnace by chemical vapor deposition (CVD). The mixture of pure zinc oxide (99.9999%) and graphite powder (molar ratio of 1:1) were loaded in an alumina boat. Sapphire chips with (110) orientation were placed above the source powder as the collecting substrates. The boat was then placed at the center of the quartz tube and inserted into a rapid heating furnace. The system was purged of contaminants with argon gas for more than ten minutes. After this, the growth carrier gas argon was maintained at 200 sccm flow. And the furnace was heated up to 1050 °C in 20 min and then the oxygen (3.0 sccm) was introduced as the reactive gas. The reaction proceeded for 30 min, after which the system was cooled down to room temperature naturally and the substrate was covered by a layer of wax-like products.

DFT Calculation: Our calculations are based on the density functional theory (DFT) within the local density approximation (LDA), in the form of Perdew-Burke-Ernzerhof's exchange correlation functional.[37,38] All the calculations are performed using the Vienna Ab-initio Simulation Package (VASP).[39] Periodic boundary conditions were employed. Geometrical optimizations of ZnO structure are performed until the Hellmann-Feynman forces on the ions are less than 1.0×10^{-4} eV/angstrom. The plane-wave basis is used, with a cut-off of 700 eV that converges the total energy to 1 meV/atom. The Brillouin zone is sampled using $1 \times 1 \times 8$ Monkhorst-Pack **k**-point scheme.[40]

Electrodynamics Simulation: The 2D partial differential equation is solved by finite element method implemented in Comsol Multiphysics. Parameters in equation are set to be: the mobility of exciton in ZnO 200 $cm^2\ s^{-1}$, temperature 5.5 K. The lifetime of exciton varies in terms of the bandgap, which in our system ranges from 160 ps (belly side) to 280 ps (back side). The PL pulse in time-dependent simulation is a Gaussian distribution with the time evolution, of which the standard deviation is set to 0.1 ps. Non-flux boundary conditions of belly and back side of the microwire are used, while symmetrical boundary condition is imposed in other two boundaries.

Standard 4PB and3PB ZnO Microwires Tests: A series SU8 (SU-8, 2015) pillars array, with the diameter of 6.0 um and height of 15.0 um, respectively, were fabricated on a Si substrate by photolithography and developing technology. First, spin coat the SU8 photoresist on the Si substrate (500 rpm for 10s and then 3000 rpm for 60s). Second, heat the SU8 photoresist (65°C for 1min and then 95°C for 3min). Third, the wafer was exposed under the UV lamp (12 s, 13 mW cm^{-2}) with a pre-designed graph as the mask template. Finally, the wafer was developed by developer solution. After that, micromanipulation was utilized to transfer an individual ZnO microwire with diameter larger than 1.0 μm (much more larger than the exciton diffusion length of ZnO at 5.5K (~100 nm)[41] and the length over hundreds of micrometers of interesting from the growth substrate on to the prearranged substrate under an optical microscope by using two needle-shaped glass tips. The ZnO microwire was manipulated to suspend over the substrate by sticking in the middle of four SU8 pillars, which restrict the wire in a curved shape after removing the two glass tips. According to ASTM E855–08, in the standard 4PB setup, the bending part between the two inner SU8 pillars is expected to be under a pure bending strain state. Such suspended bending deformation is elastic and the curved micro-wire can resume its original straight state once it is taken out of the SU8 pillars. The standard 3PB measurements were carried out by similar processes.

CL Measurements: To obtain the optimum spatial resolution with best signal-to-noise ratio, an electron beam (with beam current of about 0.353 nA) was accelerated at 10 KV voltage, which results in the effective interaction of electron beam in ZnO ranging about 100 nm (with 90% power in this region, as supported by Monte Carlo simulation[42]. The CL spectra were carefully collected step by step along the radial direction across the diameter of the ZnO microwires from outer side to inner side by CL spectroscopy (Gatan monocle 3+) at liquid helium temperature (5.5K). The CL spectra were recorded by CCD (Charge Coupled Device) with a scanning range of 300 to 450 nm with spectral resolution of about 0.5 nm. The line-scanning step size was set at about 70–100 nm.

Supporting Information

Supporting Information is available from the Wiley Online Library or from the author.

Acknowledgements

This work is supported by NSFC (Grant No. 11234001, 11174009, 91023026), the National 973 Programs of China (2013CB921900, 2012CB619402, 2009CB623703). The authors are also grateful to the financial support from the Sino-Swiss Science and Technology Cooperation Program (2010DFA01810), and NSFC/RGC (N HKUST615/06). J.L. acknowledges support by NSF DMR-1008104 and DMR-1120901. We thank Profs. Zhonglin Wang and Junren Shi, and Dr Xiaofeng Qian and Mr Ran Duan for useful discussions. D.P.Y. initiated and guided the project. J.F., J.L. and W.L.G provided the theoretical analysis, and C.S. carried out the simulation and the modelling. X.W.F. designed and performed the experiments with Q.F., X.L.Z., R.Z., C.P.L. and J.X.. X.W.F., C.S. and J.F. analysed the data and

wrote the paper. All authors contributed to discussion of the results and reviewed the manuscript. The authors declare no competing financial interests.

Received: October 10, 2013
Revised: November 8, 2013
Published online: January 27, 2014

[1] W. Shockley, H. J. Queisser, *J. Appl. Phys.* **1961**, *32*, 510.
[2] A. De Vos, *J. Phys. D* **2000**, *13*, 839.
[3] B. R. Henry, W. R. A. Greenlay, *J. Chem. Phys.* **1980**, *72*, 5516.
[4] S. A. Mcdonald, G. Konstantatos, S. Zhang, P. W. Cyr, E. J. D. Klem, L. Levina, E. H. Sargent, *Nature Mater.* **2005**, *4*, 138.
[5] Z. Kang, C. H. A. Tsang, N. B. Wong, Z. Zhang, S. T. Lee, *J. Am. Chem. Soc.* **2007**. *129*, 12090.
[6] M. Ieong, B. Doris, J. Kedzierski, K. Rim, M. Yang, *Science* **2004**, *306*, 2057.
[7] S. S. Kwon, W. K. Hong, G. Jo, J. Maeng, T. W. Kim, S. Song, T. Lee, *Adv. Mater.* **2008**, *20*, 4557.
[8] T. Zhu, J. Li, *Progress in Materials Science* **2010**, *55*, 710.
[9] C. Lee, X. Wei, J. W. Kysar, J. Hone, *Science* **2008**, *321*, 385.
[10] T. Zhu, J. Li, S. Ogata, S. Yip, *MRS Bull.* **2009**, *34*, 167.
[11] X. Han, L. Kou, X. Lang, J. Xia, N. Wang, R. Qin, J. Lu, J. Xu, Z. Liao, X. Zhang, *Adv. Mater.* **2009**, *21*, 4937.
[12] C. Dietrich, M. Lange, F. Klupfel, H. Von Wenckstern, R. Schmidt-Grund, M. Grundmann, *Appl. Phys. Lett.* **2011**, *98*, 031105.
[13] H. Xue, N. Pan, M. Li, Y. Wu, X. Wang, J. Hou, *Nanotech.* **2010**, *21*, 215701.
[14] X. Han, L. Kou, Z. Zhang, Z. Zhang, X. Zhu, J. Xu, Z. Liao, W. Guo, D. Yu, *Adv. Mater.* **2012**, *24*, 4707.
[15] S. Xu, W. Guo, S. Du, M. M. T. Loy, N. Wang, *Nano Lett.* **2012**, *12*, 5802.
[16] Z. Liao, H. C. Wu, Q. Fu, X. Fu, X. Zhu, J. Xu, I. V. Shvets, Z. Zhang, W. Guo, Y. Leprince-Wang, D. Yu, *Scientific Reports* **2012**, *2*.
[17] Q. Fu, Z. Y. Zhang, L. Kou, P. Wu, X. Han, X. Zhu, J. Gao, J. Xu, Q. Zhao, W. Guo, *Nano Res.* **2011**, *4*, 308.
[18] B. Wei, K. Zheng, Y. Ji, Y. F. Zhang, Z. Zhang, and X. Han, *Nano Lett.* **2012**, *12*, 4595.
[19] G. Signorello, S. Karg, M. T. Björk, B. Gotsmann, H. Riel, *Nano Lett.* **2013**, *13*, 917.
[20] Y. Qin, X. Wang, Z. L. Wang, *Nature* **2008**, *451*, 809.
[21] Z. L. Wang and J. Song, *Science* **2006**, *312*, 242.
[22] J. Song, J. Zhou, Z. L. Wang, *Nano Lett.* **2006**, *6*, 1656.
[23] Q. Yang, W. Wang, S. Xu, Z. L. Wang, *Nano Lett.* **2011**, *11*, 4012.
[24] J. Bardeen, W. Shockley, *Phys. Rev.* **1950**, *80*, 72.
[25] Y. Zhang, *Phys. Rev. B* **1994**, *49*, 14352.
[26] M. Cazzanelli, F. Bianco, E. Borga, G. Pucker, M. Ghulinyan, E. Degoli, E. Luppi, V. Véniard, S. Ossicini, D. Modotto, *Nature Mater.* **2011**, *11*, 148.
[27] J. Feng, X. Qian, C. W. Huang, J. Li, *Nature Photon.* **2012**, *6*, 866.
[28] T. Gruber, G. Prinz, C. Kirchner, R. Kling, F. Reuss, W. Limmer, A. Waag, *J. Appl. Phys.* **2004**, *96*, 289.
[29] W. Shan, W. Walukiewicz, J. AgerIII, K. Yu, Y. Zhang, S. Mao, R. Kling, C. Kirchner, A. Waag, *Appl. Phys. Lett.* **2005**, *86*, 153117.
[30] A. Mang, K. Reimann, S. Rübenacke, *Solid State Commun.* **1995**, *94*, 251.
[31] X. Fu, Z. Liao, R. Liu, J. Xu, D. Yu, *ACS Nano* **2013**, *7*, 8891.
[32] B. K. Meyer, H. Alves, D. M. Hofmann, W. Kriegseis, D. Forster, F. Bertram, J. Christen, A. Hoffmann, M. Straßburg, M. Dworzak, U. Haboeck, A. V. Rodina, *physica status solidi (b)* **2004**, *241*, 231.
[33] D. Hamby, D. Lucca, M. Klopfstein, G. Cantwell, *J. Appl. Phys.* **2003**, *93*, 3214.
[34] T. Nobis, E. M. Kaidashev, A. Rahm, M. Lorenz, M. Grundmann, *Phys. Rev. Lett.* **2004**, *93*, 103903.
[35] X. Wang, J. Zhou, J. Song, J. Liu, N. Xu, Z. L. Wang, *Nano Lett.* **2006**, *6*, 2768.
[36] S. Yang, L. Wang, X. Tian, Z. Xu, W. Wang, X. Bai, E. Wang, *Adv. Mater.* **2012**, *24*, 4676.
[37] J. P. Perdew, K. Burke, M. Ernzerhof, *Phys. Rev. Lett.* **1996**, *77*, 3865.
[38] Y. Hu, Y. Chang, P. Fei, R. L. Snyder, Z. L. Wang, *ACS Nano* **2010**, *4*, 1234.
[39] G. Kresse, J. Furthmuller, *Phys. Rev. B* **1996**, *54*, 11169.
[40] H. J. Monkhorst, J. D. Pack, *Phys. Rev. B* **1976**, *13*, 5188.
[41] J. Yoo, G. C. Yi, L. S. Dang, *Small* **2008**, *4*, 467.
[42] J. Xu, L. Chen, L. Yu, H. Liang, B. Zhang, K. M. Lau, *J. Electron. Mater.* **2007**, *36*, 1144.